nature physics

SUPPLEMENTARY INFORMATION

DOI: 10.1038/NPHYS4295

In the format provided by the authors and unedited.

# Fermi surface in the absence of a Fermi liquid in the Kondo insulator $SmB_6$

M. Hartstein[1*], W. H. Toews[2*], Y.-T. Hsu[1*], B. Zeng[3], X. Chen[1], M. Ciomaga Hatnean[4], Q. R. Zhang[3], S. Nakamura[5], A. S. Padgett[6], G. Rodway-Gant[1,7], J. Berk[1], M. K. Kingston[1], G. H. Zhang[1,8], M. K. Chan[9], S. Yamashita[10], T. Sakakibara[5], Y. Takano[6], J.-H. Park[3], L. Balicas[3], N. Harrison[9], N. Shitsevalova[11], G. Balakrishnan[4], G. G. Lonzarich[1], R. W. Hill[2], M. Sutherland[1†], & Suchitra E. Sebastian[1†]

[1]Cavendish Laboratory, Cambridge University, Cambridge CB3 OHE, UK,
[2]Department of Physics and Astronomy, University of Waterloo, Waterloo, ON N2L 3G1, Canada,
[3]National High Magnetic Field Laboratory, Tallahassee, FL 32310, USA,
[4]Department of Physics, University of Warwick, Coventry, CV4 7AL, UK,
[5]The Institute for Solid State Physics, The University of Tokyo, Kashiwa, Chiba 277-8581, Japan,
[6]Department of Physics, University of Florida, Gainesville, FL 32611, USA,
[7]Department of Physics, Oxford University, Oxford, OX1 3PU, UK,
[8]Department of Physics, Massachusetts Institute of Technology, Cambridge, MA 02139, USA,
[9]National High Magnetic Field Laboratory, LANL, Los Alamos, NM 87504, USA,
[10]Department of Chemistry, Osaka University, Toyonaka, Osaka 560-0043, Japan,
[11]The National Academy of Sciences of Ukraine, Kiev 03680, Ukraine.

*These authors contributed equally to this work.
†To whom correspondence should be addressed; E-mail: mls41@cam.ac.uk or ses59@cam.ac.uk.

September 26, 2017

**Estimate of the magnetic breakdown field.** We consider the possibility of magnetic breakdown, which would create large breakdown cyclotron orbits at sufficiently high magnetic fields. We find an estimate for the magnetic field where magnetic breakdown would occur by using the Blount criteria [1], given by

$$H_{breakdown} = \frac{\pi\hbar}{e}\left(\frac{k_g^3}{a_r + b_r}\right)^{1/2} \quad (1)$$

Here $1/a_r$ and $1/b_r$ are the radii of curvature of the two closest Fermi surface sections (neighbouring ellipsoids) and $k_g$ is their separation in reciprocal space. Applying this expression for the 300 T ellipsoids we have a separation of one quarter of the Brillouin zone, $k_g \approx 3.8$ nm$^{-1}$, and a radius of curvature $1/a_r = 1/b_r \approx 1$ nm$^{-1}$, taken from Table 1. This gives a giant magnetic breakdown field of $\approx 11000$ T, which is well above the magnetic field we access in the laboratory.

**Static metallic islands considered as a possible explanation for quantum oscillations.** A possibility to be considered is that static metallic islands such as those induced by frozen-in disorder are present in Kondo insulating $SmB_6$. In order to explain our results, however, a major fraction of the crystal would need to comprise such metallic islands, given the comparable size of measured quantum oscillations in the infinite field quantum limit in $SmB_6$ to metallic $LaB_6$ (Figs. 1d-e); yet no signature of significant metallic inclusions is indicated in $SmB_6$, which would be expected to be manifested for instance as a reduction in charge gap size [2], or finite electrical conductivity in measurements such as electrical transport or optical conductivity measurements [3, 4, 5, 6, 7, 8, 9, 10, 11, 12]. The high quality of single crystals measured in this study is confirmed by the measured phonon peak in thermal conductivity at 10 K, which is significantly larger than in previous generations of single crystals [13] (Supplementary Fig. S11). Furthermore, a static magnetic moment would be expected to accompany metallic behaviour in

$SmB_6$, as predicted within the traditional Kondo lattice model [14], and indeed observed in the case of metallic $SmB_6$ under pressure [15, 16, 17]. In contrast, single crystals of $SmB_6$ from similar growths that produced the single crystals on which quantum oscillation measurements are performed show no evidence for a static magnetic moment in measurements such as muon spin resonance [18], neutron scattering [19], nuclear magnetic resonance [20] and magnetisation (Supplementary Fig. S2).

**Absence of quantum oscillations in organic spin liquids.** In the organic spin liquid materials, $EtMe_3Sb[Pd(dmit)_2]_2$ and $\kappa$-$(BEDT\text{-}TTF)_2Cu_2(CN)_3$, the lack of evidence of quantum oscillatory effects might seem at first puzzling within a spin liquid scenario [21, 22]. One possibility to explain the lack of observed quantum oscillations in the organic spin liquid materials is the formation of Condon domains, as proposed in ref. [21]. Another possibility is due to the large size of the charge gap $\approx 50$ meV in these materials, compared to the size of the charge gap $\approx 3$ meV in the case of Kondo insulating $SmB_6$ [2, 3, 4, 5, 6, 7, 9, 10, 11, 12]. The mechanism of diamagnetism arising from virtual charge fluctuations would result in an enhanced damping of the quantum oscillation amplitude compared to the infinite field limit; consequently, a larger charge gap would render such oscillations even more challenging to observe experimentally. The positioning of $SmB_6$ closer to the edge of the insulator-metal transition would result in enhanced virtual charge fluctuations, increasing the expected size of time-averaged diamagnetism and associated quantum oscillations in an applied magnetic field. Furthermore, solely high quantum oscillation frequencies corresponding to the single band Fermi surface are expected in the organic spin liquids, with a considerably higher effective mass expected from the significantly larger size of the linear specific heat coefficient [23, 24, 25] in the organic spin liquids compared to $SmB_6$, which would make quantum oscillations more challenging to detect. The situation is therefore rendered more conducive to the observation of quantum oscillations in Kondo insulating $SmB_6$ within the theoretical scenario of a neutral Fermi surface.

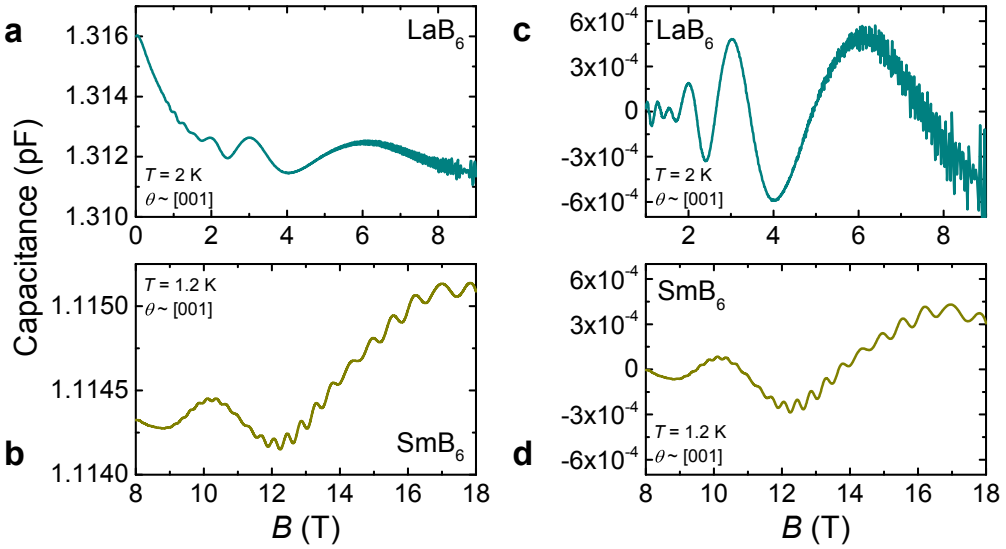


Figure S1: **a**, Capacitive torque as a function of magnetic field measured in $LaB_6$, showing the background magnetic torque and quantum oscillations that appear at high fields. **b**, Capacitive torque as a function of magnetic field measured flux-grown $SmB_6$, measured with an identical setup, showing the background magnetic torque and quantum oscillations that appear at high fields. **c**, Quantum oscillations as a function of magnetic field measured in $LaB_6$, corresponding to a low exponential damping factor $\exp(-B_0/B)$ where $B_0 \approx 1$ T for the lowest frequency. **d**, Quantum oscillations as a function of magnetic field measured in $SmB_6$, corresponding to a significantly higher exponential damping factor $\exp(-B_0/B)$ where $B_0 \approx 30$ T for the lowest frequency. To obtain **c** and **d** a smooth 3rd order and 2nd order polynomial background was subtracted respectively.

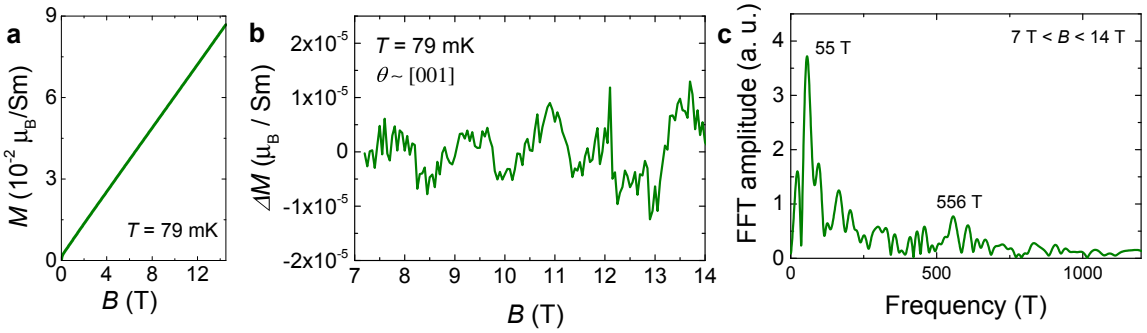


Figure S2: **a**, The magnetisation measured for floating zone-grown $SmB_6$ in a superconducting magnet using capacitive Faraday magnetometry shows weak featureless magnetic susceptibility. **b**, Quantum oscillations observed in the magnetisation on subtraction of a 4th order polynomial background. **c**, The frequencies found from the Fourier transform are similar to the characteristic frequencies in Fig. 1b.

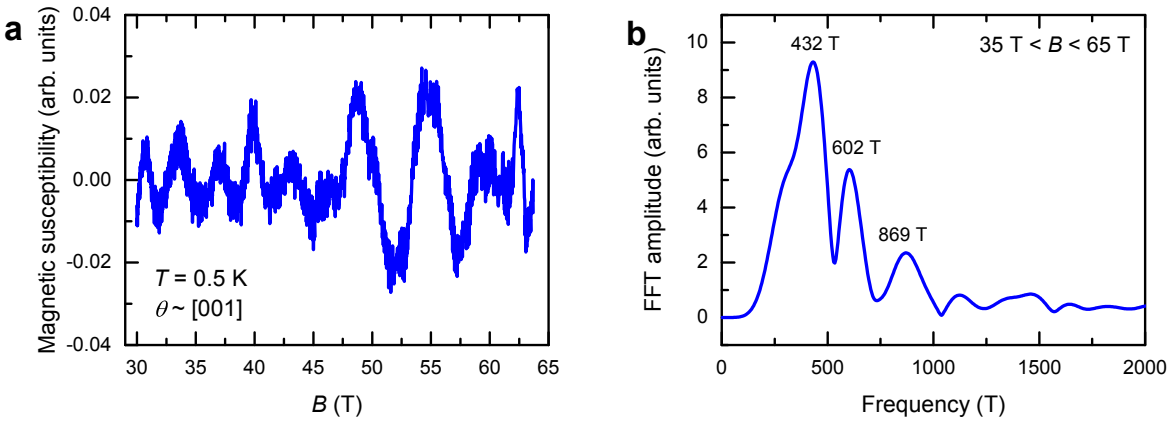


Figure S3: **a**, Quantum oscillations extracted from the magnetic susceptibility measured in pulsed magnetic fields for floating zone-grown $SmB_6$ by averaging four consecutive pulses. **b**, The Fourier transform reveals frequencies that are similar to the characteristic frequencies denoted by $\rho$ and $\epsilon$ in Fig. 1b.

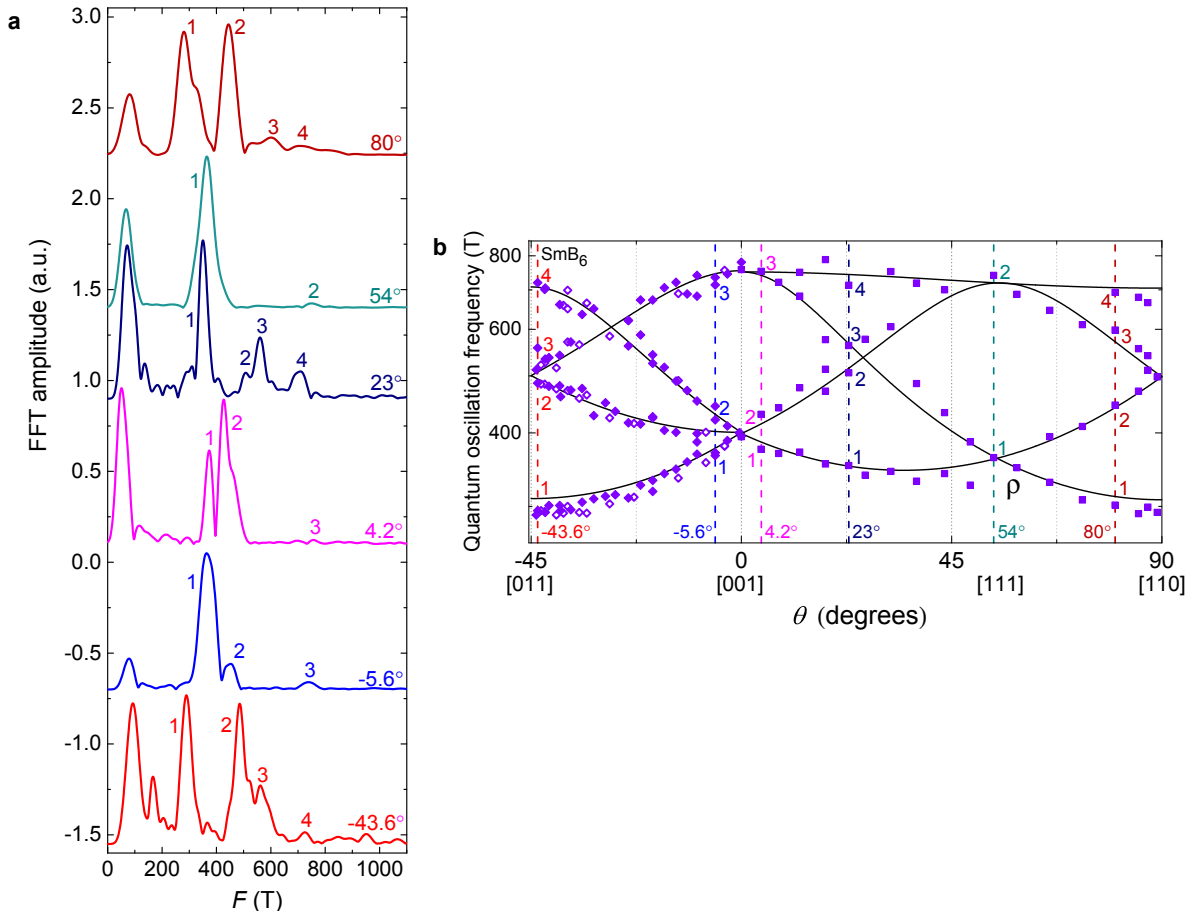


Figure S4: **a**, The FFTs of field sweeps taken at different angles for flux-grown $SmB_6$, used to identify the $\rho$ frequencies shown in main text Fig. 1b, and also indicated in **b** by vertical dashed lines for each shown angle. The observation of all frequency branches over the entire angular range provides evidence for a three-dimensional Fermi surface model, rather than a two-dimensional Fermi surface model, in which case the Fermi surface orbits would be open for certain tilt angles.

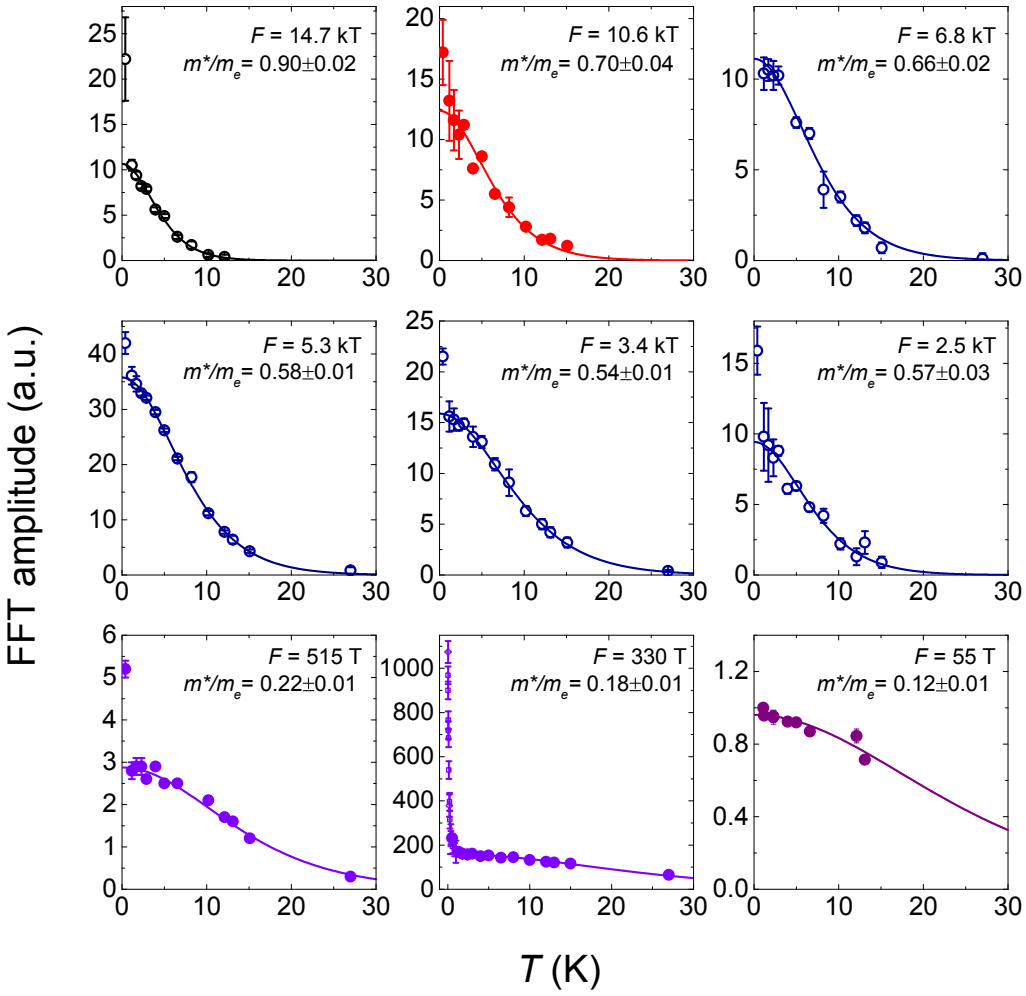


Figure S5: The temperature dependence of quantum oscillation amplitude for each of the quantum oscillation frequencies in floating zone-grown $SmB_6$ observed for a magnetic field applied along ≈ [110] for temperatures down to 20 mK for the dominant $F = 330$ T frequency, and down to 0.4 K for all other frequencies. Effective masses are extracted for a magnetic field window of 21 to 40 T and a temperature range of 1 K to 30 K, while the temperature dependence is found to adhere to Lifshitz-Kosevich behaviour down to ≈ 1 K. For $T \leq 1$ K, an anomalous increase in quantum oscillation amplitude that displays a marked departure from the Lifshitz-Kosevich form is observed in the majority of observed quantum oscillation frequencies, The error in the amplitude corresponds to the noise floor of the Fourier transform.

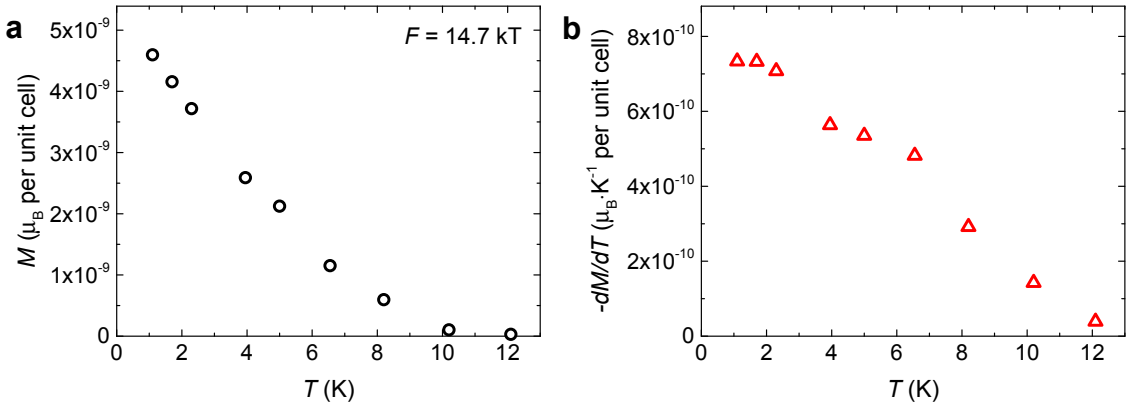


Figure S6: **a**, The size of the oscillatory magnetisation arising from the highest frequency oscillations measured in floating zone-grown $SmB_6$ between magnetic fields of 21 to 40 T applied along $\approx$ [110] (also shown in Fig. S5). **b**, The derivative of the amplitude of the oscillatory magnetisation with respect to temperature.

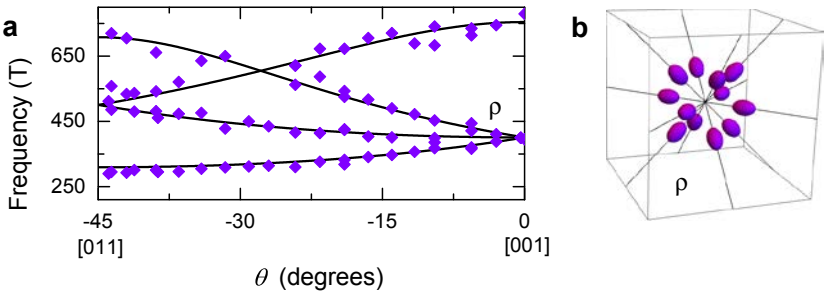


Figure S7: **a**, A magnified view of the measured angular dependence of the low frequency quantum oscillation branches (labelled $\rho$) shown in Fig. 1b of the main text, in a single crystal of flux-grown $SmB_6$. Four distinct branches are observed, with angular dependences for the [011]-[001] rotation plane that display the signature characteristics of an ellipsoidal Fermi surface model [1], corresponding to twelve ellipsoidal pockets aligned along the $<110>$ directions, as illustrated in **b**.

Table S1: Measured dHvA frequencies and effective masses, and the relative ratios of the semi-principal axes of the ellipsoidal Fermi surfaces denoted by $a$, $b$ and $c$ as obtained from fitting to the angular dependence of the quantum oscillatory magnetisation of $SmB_6$ shown in Fig. 1b of the main text and in ref. [2]. These quantities enable the estimation of the contribution of each Fermi surface sheet to the linear specific heat coefficient $\gamma$, to be compared with the value obtained from the heat capacity.

| Sheet | $F_{min}$ (T) | $m^*$ ($m_e$) | $ak_0$ (nm$^{-1}$) | $b/a$ | $c/a$ | $\gamma$ (mJ·mol$^{-1}$·K$^{-2}$) |
|---|---|---|---|---|---|---|
| $\alpha$ | 7750(90) | 0.70(4) | 4.85(3) | 1 | 1.36(2) | 3.1(4) |
| $\rho$ | 309(14) | 0.18(1) | 1.00(2) | 0.94(4) | 2.3(1) | 1.1(3) |
| $\rho'$ | 31(6) | 0.12(1) | 0.23(2) | 1.2(2) | 3.9(5) | 0.3(2) |

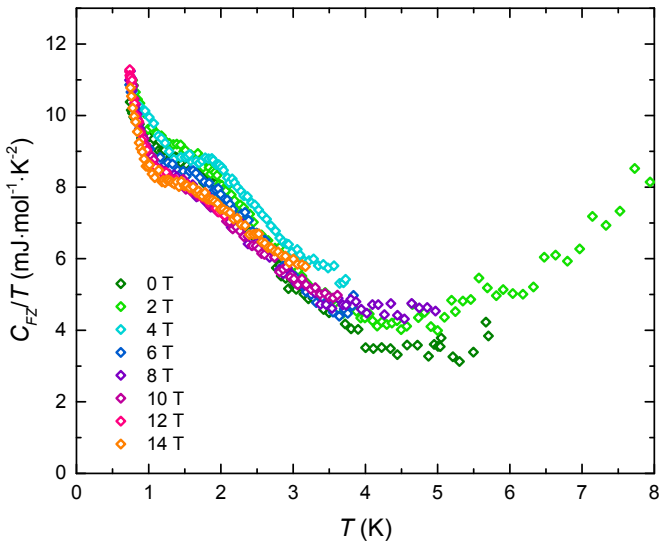


Figure S8: Measured specific heat capacity of $SmB_6$ in magnetic fields up to 14 T and down to 700 mK in temperature for the floating zone-grown crystal (for which zero magnetic field data are shown in the inset to Fig. 2a of the main text).

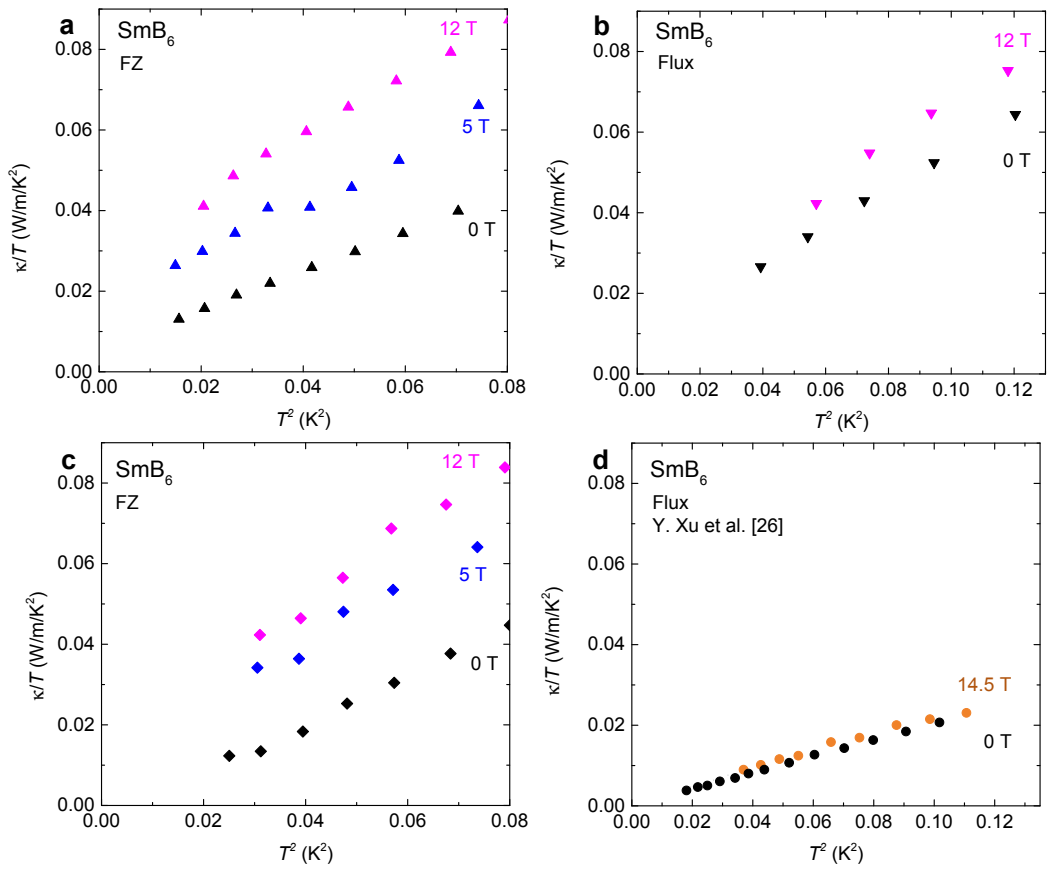


Figure S9: Thermal conductivity of floating zone-grown single crystals (**a-b**) and a flux-grown single crystal (**c**) of $SmB_6$; also shown in **d** is the thermal conductivity of a flux-grown single crystal from ref. [26]. The thermal gradient is applied along the [100] direction, with perpendicular magnetic field applied along [001].

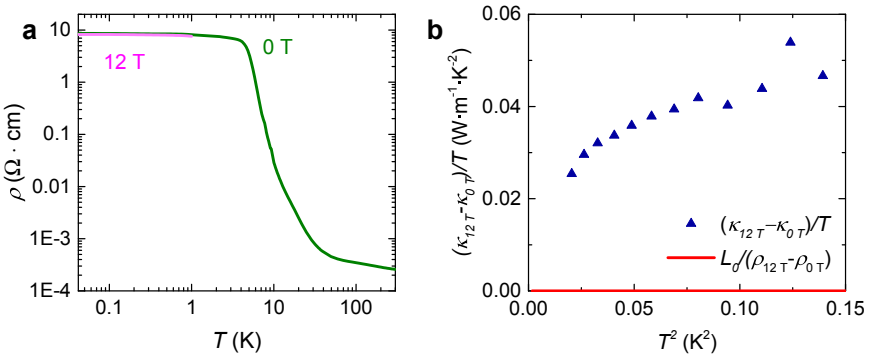


Figure S10: **a**, Electrical resistivity, as a function of temperature at 0 T (green line) and at 12 T (pink line) measured on the same single crystal of floating zone-grown $SmB_6$ for which thermal conductivity results are reported in the main text Fig. 3a. The inverse electrical resistivity ratio between 2 K and 300 K is found to be $\approx 3 \cdot 10^4$. The current is applied along the [100] direction, with perpendicular magnetic field applied along [001]. **b**, Comparison of the enhancement in low temperature thermal conductivity at 12 T compared to 0 T, with that expected from the enhancement in the electrical conductivity based on the Wiedemann-Franz law (red line). The observed enhancement in low temperature thermal conductivity is found to be a factor of $10^4$ larger than the Wiedemann-Franz expectation.

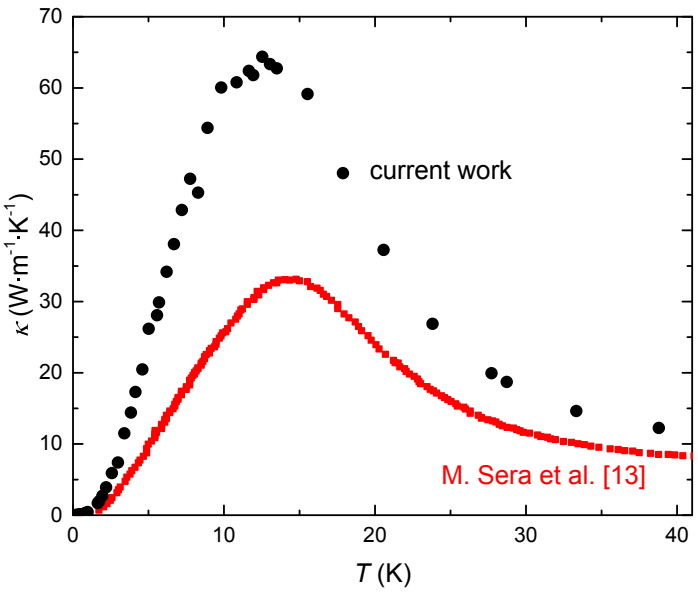


Figure S11: The large size of the thermal conductivity peak in a floating zone-grown $SmB_6$ crystal reported in this work in zero magnetic field, compared to that of a previously reported $SmB_6$ sample [13] indicates the high quality of our crystals, which are characterised by longer phonon mean free paths.

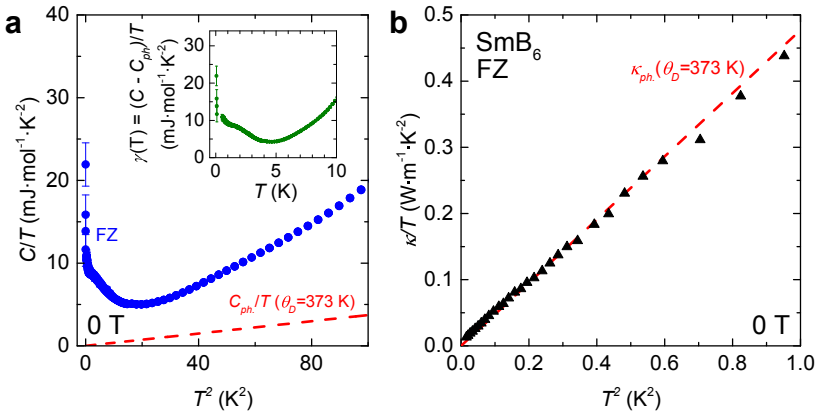


Figure S12: **a**, Measured specific heat capacity of $SmB_6$, also shown in main text Fig. 2, and the phonon contribution for a Debye temperature of $\Theta_D = 373$ K, the value calculated from elastic constants for $SmB_6$ [27]. The inset shows the linear coefficient $\gamma$, which is found to be finite at low temperatures, unexpected for an insulator. **b**, Thermal conductivity of a floating zone-grown single crystal in zero magnetic field, compared with the thermal conductivity calculated in the low temperature limit for phonon transport for a Debye temperature of $\Theta_D = 373$ K [27]; good agreement is seen at low temperatures.

# References


[1] Shoenberg, D. *Magnetic Oscillations in Metals* (Cambridge University Press, 1984).

[2] Tan, B. S. *et al.* Unconventional Fermi surface in an insulating state. *Science* **349**, 287–290 (2015).

[3] Kim, D. J. *et al.* Surface Hall Effect and Nonlocal Transport in $SmB_6$: Evidence for Surface Conduction. *Scientific Reports* **3**, 3150 (2013).

[4] Wolgast, S. *et al.* Low-temperature surface conduction in the Kondo insulator $SmB_6$. *Physical Review B* **88**, 180405 (2013).

[5] Zhang, X. *et al.* Hybridization, Inter-Ion Correlation, and Surface States in the Kondo Insulator $SmB_6$. *Physical Review X* **3**, 011011 (2013).

[6] Hatnean, M. C., Lees, M. R., Paul, D. M. & Balakrishnan, G. Large, high quality single-crystals of the new Topological Kondo Insulator, $SmB_6$. *Scientific Reports* **3**, 3071 (2013).

[7] Phelan, W. *et al.* Correlation between Bulk Thermodynamic Measurements and the Low-Temperature-Resistance Plateau in $SmB_6$. *Physical Review X* **4**, 031012 (2014).

[8] Menth, A., Buehler, E. & Geballe, T. H. Magnetic and Semiconducting Properties of $SmB_6$. *Physical Review Letters* **22**, 295 (1969).

[9] Nanba, T. *et al.* Gap state of $SmB_6$. *Physica B: Condensed Matter* **186**, 440–443 (1993).

[10] Allen, J. W., Batlogg, B. & Wachter, P. Large low-temperature Hall effect and resistivity in mixed-valent $SmB_6$. *Physical Review B* **20**, 4807 (1979).

[11] Roman, J. *et al.* Transport and magnetic properties of mixed valent $SmB_6$. *Physica B: Condensed Matter* **230**, 715–717 (1997).

[12] Gorshunov, B. *et al.* Low-energy electrodynamics of $SmB_6$. *Physical Review B* **59**, 1808 (1999).

[13] Sera, M., Kobayashi, S., Hiroi, M., Kobayashi, N. & Kunii, S. Thermal conductivity of $RB_6$ (R= Ce, Pr, Nd, Sm, Gd) single crystals. *Physical Review B* **54**, R5207–R5210 (1996).

[14] Coleman, P., Pépin, C., Si, Q. & Ramazashvili, R. How do Fermi liquids get heavy and die? *Journal of Physics: Condensed Matter* **13**, R723 (2001).

[15] Cooley, J., Aronson, M., Fisk, Z. & Canfield, P. High pressure insulator-metal transition in $SmB_6$. *Physica B: Condensed Matter* **199200**, 486 – 488 (1994).

[16] Gabáni, S. *et al.* Pressure-induced Fermi-liquid behavior in the Kondo insulator $SmB_6$: Possible transition through a quantum critical point. *Physical Review B* **67**, 172406 (2003).

[17] Barla, A. *et al.* High-pressure ground state of $SmB_6$: electronic conduction and long range magnetic order. *Physical Review Letters* **94**, 166401 (2005).

[18] Biswas, P. K. *et al.* Low-temperature magnetic fluctuations in the Kondo insulator $SmB_6$. *Physical Review B* **89**, 161107 (2014).

[19] Fuhrman, W. T. *et al.* Interaction Driven Subgap Spin Exciton in the Kondo Insulator $SmB_6$. *Physical Review Letters* **114**, 036401 (2015).

[20] Caldwell, T. *et al.* High-field suppression of in-gap states in the Kondo insulator $SmB_6$. *Physical Review B* **75**, 075106 (2007).

[21] Motrunich, O. I. Orbital magnetic field effects in spin liquid with spinon Fermi sea: Possible application to $\kappa$-$(ET)_2Cu_2(CN)_3$. *Physical Review B* **73**, 155115 (2006).

[22] Lee, S.-S. & Lee, P. A. U(1) gauge theory of the Hubbard model: Spin liquid states and possible application to $\kappa$-(BEDT- TTF)$_2$Cu$_2$(CN)$_3$. *Physical Review Letters* **95**, 036403 (2005).

[23] Yamashita, M. *et al.* Highly mobile gapless excitations in a two-dimensional candidate quantum spin liquid. *Science* **328**, 1246–1248 (2010).

[24] Yamashita, M., Shibauchi, T. & Matsuda, Y. Thermal-Transport Studies on Two-Dimensional Quantum Spin Liquids. *ChemPhysChem* **13**, 74–78 (2012).

[25] Yamashita, M. *et al.* Thermal-transport measurements in a quantum spin-liquid state of the frustrated triangular magnet $\kappa$-(BEDT-TTF)$_2$Cu$_2$ (CN)$_3$. *Nature Physics* **5**, 44–47 (2009).

[26] Xu, Y. *et al.* Bulk Fermi Surface of Charge-Neutral Excitations in $\mathrm{SmB_6}$ or Not: A Heat-Transport Study. *Physical Review Letters* **116**, 246403 (2016).

[27] Smith, H. *et al.* Experimental study of lattice dynamics in $\mathrm{LaB_6}$ and $\mathrm{YbB_6}$. *Solid State Communications* **53**, 15–19 (1985).